Pannexin-1 mediates fluid shear stress-sensitive purinergic signaling and cyst growth in polycystic kidney disease

Verschuren, E.H.J.; Rigalli, J.P.; Castenmiller, C.; Rohrbach, M.U.; Bindels, R.J.M.; Peters, D.J.M.; ... ; Hoenderop, J.G.J.

Received: 15 November 2019 | Revised: 7 February 2020 | Accepted: 1 March 2020

DOI: 10.1096/fj.201902901R

RESEARCH ARTICLE

THE FASEB JOURNAL

Pannexin-1 mediates fluid shear stress-sensitive purinergic signaling and cyst growth in polycystic kidney disease

Eric H. J. Verschuren[1] | Juan P. Rigalli[1] | Charlotte Castenmiller[1] | Meike U. Rohrbach[1] | René J. M. Bindels[1] | Dorien J. M. Peters[2] | Francisco J. Arjona[1] | Joost G. J. Hoenderop[1]

[1]Department of Physiology, Radboud Institute for Molecular Life Sciences, Radboud University Medical Center, Nijmegen, the Netherlands

[2]Department of Human Genetics, Leiden University Medical Center, Leiden, the Netherlands

Correspondence
Joost G. J. Hoenderop, Department of Physiology (286), Radboud Institute for Molecular Life Sciences, Radboud University Medical Center, P.O. Box 9101, 6500 HB Nijmegen, the Netherlands.
Email: Joost.Hoenderop@radboudumc.nl

Funding information
Nierstichting (Dutch Kidney Foundation), Grant/Award Number: 15OP03; Nederlandse Organisatie voor Wetenschappelijk Onderzoek (NWO), Grant/Award Number: NWO VICI 016.130.668

Abstract

Tubular ATP release is regulated by mechanosensation of fluid shear stress (FSS). Polycystin-1/polycystin-2 (PC1/PC2) functions as a mechanosensory complex in the kidney. Extracellular ATP is implicated in polycystic kidney disease (PKD), where PC1/PC2 is dysfunctional. This study aims to provide new insights into the ATP signaling under physiological conditions and PKD. Microfluidics, pharmacologic inhibition, and loss-of-function approaches were combined to assess the ATP release in mouse distal convoluted tubule 15 (mDCT15) cells. Kidney-specific *Pkd1* knockout mice (iKsp-*Pkd1*$^{-/-}$) and zebrafish *pkd2* morphants (*pkd2*-MO) were as models for PKD. FSS-exposed mDCT15 cells displayed increased ATP release. Pannexin-1 inhibition and knockout decreased FSS-modulated ATP release. In iKsp-*Pkd1*$^{-/-}$ mice, elevated renal pannexin-1 mRNA expression and urinary ATP were observed. In *Pkd1*$^{-/-}$ mDCT15 cells, elevated ATP release was observed upon the FSS mechanosensation. In these cells, increased pannexin-1 mRNA expression was observed. Importantly, pannexin-1 inhibition in *pkd2*-MO decreased the renal cyst growth. Our results demonstrate that pannexin-1 channels mediate ATP release into the tubular lumen due to pro-urinary flow. We present pannexin-1 as novel therapeutic target to prevent the renal cyst growth in PKD.

KEYWORDS

ATP, fluid shear stress, pannexin-1, polycystin-1, purinergic signaling

Abbreviations: Abcc6, ATP binding cassette subfamily c member 6; BB-FCF, brilliant blue-FCF; Cx30, connexin30; Cx30.3, connexin30.3; Cx37, connexin37; Entpd2, ectonucleoside triphosphate diphosphohydrolase 2; Entpd3, ectonucleoside triphosphate diphosphohydrolase 3; FBS, fetal bovine serum; FSS, fluid shear stress; Gapdh, glyceraldehyde 3-phosphate dehydrogenase; MO, translation blocking morpholino; Nt5e, ecto-5′-nucleotidase; Panx1, pannexin-1; PC1, polycystin-1; PC2, polycystin-2; PKD, polycystic kidney disease; Pkd1, polycystic kidney disease 1; Pkd2, polycystic kidney disease 2; Ptgs2, prostaglandin-endoperoxide synthase 2.

Francisco J. Arjona and Joost G. J. Hoenderop are contributed equally to this work.

1 | INTRODUCTION

Mutations in the genes *polycystic kidney disease 1* (*PKD1*) and *polycystic kidney disease 2* (*PKD2*) lead to polycystic kidney disease (PKD). PKD is characterized by increased cell proliferation, fluid accumulation, and altered extracellular matrix synthesis in the kidney. These characteristics lead to the renal cyst formation and growth, predominantly in the distal tubules and collecting duct (CD), and ultimately to end-stage kidney disease.[1-4] PKD is one of the most common inherited renal diseases and accounts for ~10% of all patients on renal replacement therapy worldwide.[5,6] The *Pkd1* gene encodes for the protein polycystin-1 (PC1), which locates to the primary cilium and plasma membrane of renal tubular epithelial cells. PC1 forms a complex with polycystin-2 (PC2, encoded by *Pkd2*), which is a nonselective cation channel.[7-11] PC1 is suggested to act as a mechanosensor of fluid shear stress (FSS) generated by pro-urine flow, regulating the physiological responses in renal tubular epithelial cells.[12,13]

In PKD, extracellular ATP plays an important role in disease progression.[14,15] Under physiological conditions, extracellular ATP activates ionotropic P2X and metabotropic P2Y receptors at the luminal cell surface to regulate and maintain the kidney function.[16] In recent years, autocrine and paracrine effects of the purinergic signaling have been suggested to provide a detrimental acceleration of cyst growth in PKD.[17-20] It has been shown that the renal cyst fluid in PKD rats and PKD patients contains high ATP levels.[21,22] Also, cystic PKD cell cultures display increased ATP release at basal conditions.[23] Furthermore, previous studies have related purinergic receptors P2Y2 and P2X7 to cyst growth in an in vitro cystic model, and in vivo, in zebrafish and mouse PKD models.[23-26]

Thus far, translation of these findings into therapeutic applications for PKD related to purinergic signaling are limited.[24] Conversely, approaches that did reach clinical research stages for PKD involve vasopressin antagonists, mTOR inhibitors, and somatostatin analogues. However, these approaches are not a definitive curative treatment option.[1,25-29] An improved understanding of the molecular mechanisms behind ATP signaling in PKD may promote the development of novel therapeutic strategies for this disease.

ATP can be released from renal epithelial cells upon the mechanical stimulation triggered by variable pro-urine flow.[30,31] Yet, the ATP extrusion mechanisms mediating flow-sensitive ATP release as well as their regulation are not fully elucidated.[32,33] The extracellular ATP in the tubule lumen signals the apical membrane of renal cells to trigger an intracellular response which results in regulation of electrolyte and water transport.[34,35]

In this study, we aimed to disclose the mechanisms regulating the apical ATP release in renal cells upon flow sensing. To this end, the urine of healthy human volunteers and cellular and organismal kidney models were interrogated. The relevance of these mechanisms for disease progression in the context of PKD was investigated, where purinergic signaling was anticipated to play a pathologic role.

2 | MATERIALS AND METHODS

2.1 | Ethics approval

Urine samples of healthy human volunteers were collected after acute water loading experimentation in accordance with the principles expressed in the Declaration of Helsinki. All participants gave written informed consent, and the study protocol was approved by the Institutional Review Board of the Radboud University Medical Center (approval no. NL47178.091.13). The local animal experimental committee of the Leiden University Medical Center and the Commission Biotechnology in Animals of the Dutch Ministry of Agriculture approved the animal procedures performed.

2.2 | Cell culture

To assess the role of FSS on ATP release, μ-slide $I^{0.4}$ and $VI^{0.4}$ channels (Ibidi GmbH, Planegg, Germany) were used for ATP and gene expression experiments, respectively. Static ATP release was assessed using 12-well plates. Mouse distal convoluted tubule 15 (mDCT15) cells (gift from Dr Robert Hoover, Emory University, Atlanta, GA, USA), a model of the distal convoluted epithelial cell, were used in all experiments.[36] mDCT15 cells (either wild type, *Ift140*$^{-/-}$ or *Pkd1*$^{-/-}$) were seeded in the channels (μ-slide $I^{0.4}$:1.2×10^5 cells/cm^2 and μ-slide $VI^{0.4}$: 5×10^4 cells/cm^2) with DMEM/F-12 1:1 nutrient mixed media supplemented with 5% v/v fetal bovine serum (FBS, GE Healthcare, Little Chalfont, United Kingdom) and 10 μg/mL ciprofloxacin, and maintained at 37°C and 5% (v/v) CO_2. The following day, cells were serum-starved for 24 hours to induce cell differentiation. Shortly before FSS experimentation, biocompatible silicone tubing (Ø0.8 mm, Ibidi GmbH, Planegg, Germany) was connected to a peristaltic pump (ISM931C, Ismatec, Wertheim, Germany) and the microfluidic channels. During microfluidic experiments serum-free DMEM/F-12 1:1 nutrient mixed media was used.

2.3 | ATP measurements

To assess the ATP release by mDCT15 cells due to FSS, cells were exposed during 1 minute to different physiologically relevant FSS levels (ie, 0.3, 0.6, and 1.2 dyn/cm^2). Cells were also exposed to repetitive cycles of 0.3 dyn/cm^2 (1 min) followed by 1.2 dyn/cm^2 (1 min) with static intervals between

cycles of 1 to 25 minutes, thus simulating dynamic changes in the pro-urine flow.

To investigate the involvement of mTORC1 and pannexin-1 in FSS-modulated ATP release, cells were pre-incubated for 1hour with rapamycin (100 nM, Santa Cruz Biotechnology, Santa Cruz, CA, USA) and brilliant blue FCF (BB-FCF, 100 μM, Sigma-Aldrich, St. Louis, MO, USA), respectively.[37,38] In this case, during microfluidic experimentation, media was supplemented with the corresponding inhibitor. Control cells were exposed tomedia supplemented with the corresponding vehicle (DMSO or MilliQ-water, for rapamycin or BB-FCF, respectively). Flow-through was collected after 1 minute of FSS exposure and used for the ATP measurement (Figure 1A). Cell morphology after exposure to different FSS conditions was monitored by brightfield microscopy (Figure 1B).

ATP levels were determined in the (flow-through) medium, total cell lysates, and urine using the ATPlite Luminescence Assay System (Perkin Elmer, Waltham, MA, USA) according to manufacturer's instructions. A standard curve, ranging from 0.6×10^6 to 2.5×10^6 and 0.3×10^2 to 10.0×10^3 pmol/L ATP for intracellular and extracellular ATP, respectively, was used. All samples measured were within the confines of the standard curve used. ATP content in the medium and total cell lysates was corrected to the total volume and normalized to the total cell number in the corresponding channel or well. For in vitro experimentation, fold change of extracellular ATP for each condition to control is depicted. In vivo, ATP content in urine was normalized to urinary creatinine for human subjects and to urinary volume collected in 24 hours for mice.[39]

2.4 | Acute water loading

Urine samples of healthy human volunteers were collected, for ATP measurement, after acute water loading experimentation. These samples were obtained from a previously performed study and supplemented with protease inhibitors at a final concentration of 50 μM PMSF, 20 μM aprotinin, 10 μM pepstatin A, and 20 μM leupeptin, and stored at −80°C.[40] All volunteers were healthy males between the age of 25 and 35years with a body weight lower than 100kg. Subjects were asked to refrain from coffee, tea, and alcohol intake and exercise for 24 hours before and during the study. In 30 minutes, each subject ingested 20ml/kg body weight of water. Midstream urine was collected before ($t = 0$) and after water ingestion in 30 minutes intervals for up to 150 minutes. Urine samples were immediately stored at −80°C.

2.5 | Mouse experimentation

Inducible kidney-specific *Pkd1* knockout mice (iKsp-*Pkd1*$^{lox/lox}$) were used to assess the role of PC1, in vivo, in urinary ATP excretion. Tamoxifen was administered, via oral gavage, to iKsp-*Pkd1*$^{lox/lox}$ mice on postnatal days 18, 19, and 20 (PN18) to induce a kidney specific knockout of *Pkd1* (iKsp-*Pkd1*^{del}).[41] iKsp-*Pkd1*$^{lox/lox}$ mice which received no tamoxifen were considered as age and genotype-matched controls. At PN18 + 29 days, mice were placed in the metabolic cages for 24 hours to collect urine in a continuously cooled container (4°C) and stored at −20°C for ATP measurements. Finally, mice were killed by cervical dislocation. Precystic kidneys were extracted, weighed, and collected in liquid nitrogen and stored at −80°C for mRNA isolation. These samples were obtained from a previously performed study.[41]

2.6 | Gene expression analysis

To evaluate the effect of FSS on gene expression, cells in μ-slide VI$^{0.4}$ channels were exposed during 3 hours to either no flow (=static) or 0.6 dyn/cm^2 FSS (Figure 4A). After experimentation, cells were lysed and RNA was isolated using the RNeasy mini kit according to manufacturer's instructions (Qiagen, Hilden, Germany). cDNA synthesis using Molony Murine Leukemia Virus Reverse Transcriptase (Invitrogen, Carlsbad, CA, USA) and RTqPCR, using SYBR green master mix (Bio-Rad Laboratories, Hercules, CA, USA) were performed as previously described.[42] The expression of the following genes was assessed: *Abcc6*, *Cx37*, *Entpd2*, *Entpd3*, *Nt5e*, *P2rx4*, *P2rx5*, *P2rx6*, *P2rx7*, *P2ry1*, *P2ry2*, *Panx1,* and *Ptgs2*. *Gapdh* was used for each gene of interest as a reference gene and non-template controls were used during RTqPCR determinations as negative controls. Since all primers used had an efficiency of approximately 100% at the concentration (400nM) used, the relative gene expression was analyzed using the Livak method ($2^{-\Delta\Delta Ct}$) (Supporting Table S1). The RTqPCR procedures described here complied with the MIQE guidelines.

2.7 | Fura-2-based Ca^{2+} imaging

Intracellular Ca^{2+} was measured using the ratiometric dye Fura-2. Press-to-Seal silicone isolators with adhesive 24 wells (Molecular Probes, Eugene, OR, USA) were attached to a 24 × 50 mm cover glass. The wells were coated with Poly-*L*-Lysine (Sigma-Aldrich, St. Louis, MO, USA) and washed with PBS. The procedures were performed in a Ca-HT buffer (4.2mM KCl, 132mM NaCl, 1mM $MgCl_2$, 1.4mM $CaCl_2$, 5.5mM glucose, and 10mM HEPES in MilliQ). Subsequent, 15 μL of cell suspension was added to each well and incubated for 1.5 hours. About 5 μL of medium was removed and 10 μL Fura-2-AM mixture (0.3% v/v Fura-2-AM, 0.015% v/v Pluronic acid (10% v/v in Ca-HT buffer) was added and incubated for 1hr. For the conditions in which P2Y1 was

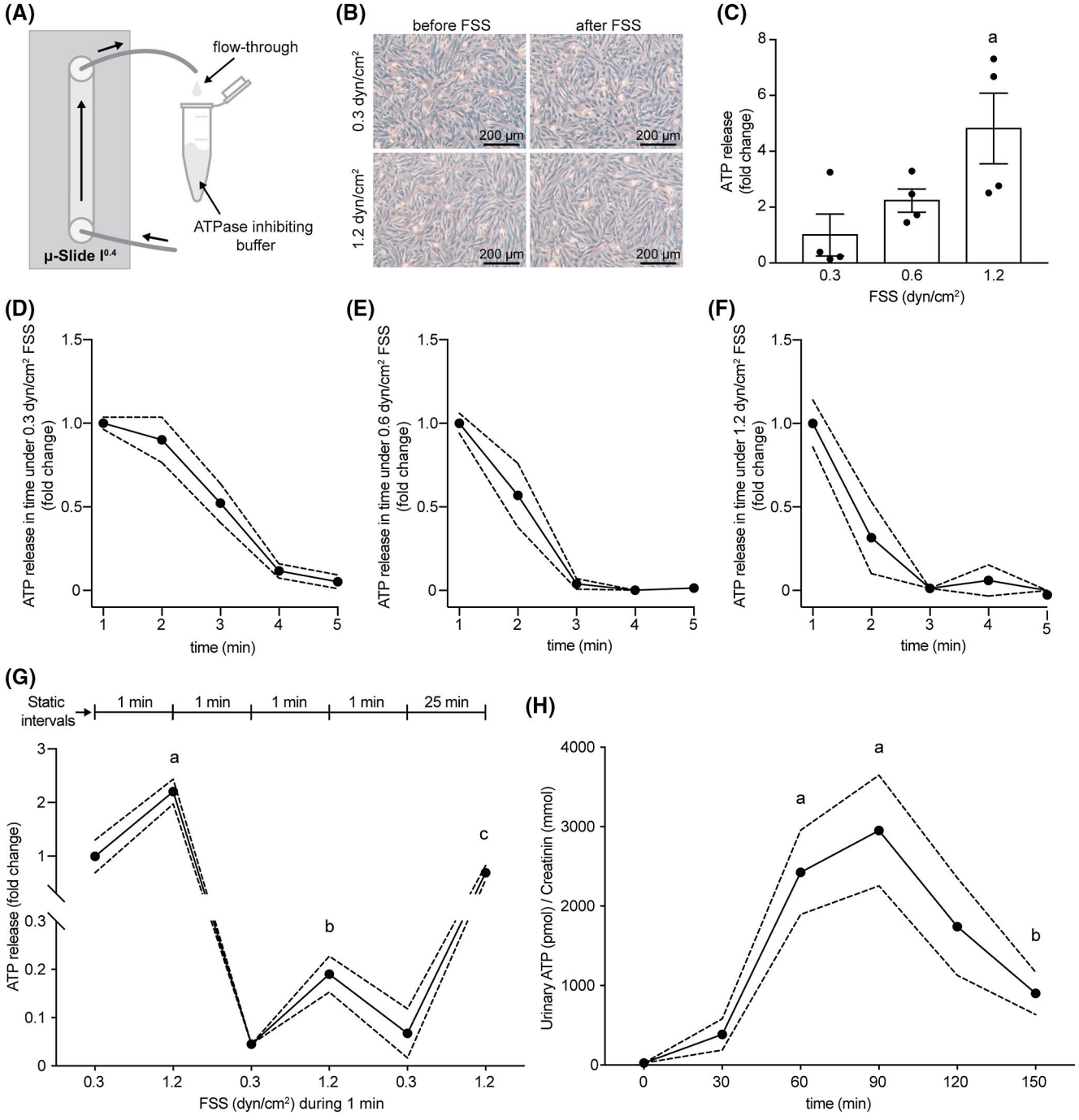

FIGURE 1 Fluid shear stress increases ATP release in vitro and in vivo. A, Schematic overview of the in vitro microfluidic set-up used to measure cellular ATP release. B, Brightfield microscopy of mDCT15 cellular morphology before and after exposure to either 0.3 and 1.2 dyn/cm^2 FSS. C, Elevated FSS-modulated ATP release in mDCT15 cells exposed to 1 minute of 0.3, 0.6, and 1.2 dyn/cm^2 FSS (n = 4), significant difference ($P < .05$) denoted with symbol a. D-F, Attenuated FSS-modulated ATP release in mDCT15 cells after repeated 1 min sampling during exposure, for 5 min in total, to 0.3, 0.6, and 1.2 dyn/cm^2 FSS, respectively (n = 4). G, Recovery of FSS-modulated ATP release after static intervals of 1 to 25 min between 1 min FSS exposure periods (0.3 to 1.2 dyn/cm^2) (n = 4), significant differences between 0.3 and 1.2 dyn/cm^2 are denoted with symbols a, b and c. H, In vivo resemblance of FSS-modulated ATP release in healthy human subjects after acute water loading (n = 7), significant differences indicating elevated urinary ATP (from $t = 0$ to $t = 60$ and $t = 90$, respectively) are denoted with symbol a, whereas significant differences indicating a decreased urinary ATP (from $t = 90$ to $t = 150$) are denoted with symbol b. Values are presented as the mean ± SEM

inhibited, MRS2500 (Tocris Bioscience, Bristol, United Kingdom) was added to the Fura-2 AM mixture at a concentration of 1 μM. One measurement per well was performed. The well was placed into a perfusion chamber mounted onto the stage of an inverted microscope (Zeiss Axiovert 200$_M$, Carl Zeiss, Jena, Germany). Intracellular Ca^{2+} was monitored

by exciting Fura-2 with monochromatic light of wavelength 340 and 380nm (Polychrome IV, TILL Photonics, Gräfelfing, Germany). Fluorescence emission light was directed by a 415DCLP dichroic mirror (Omega Optical, Brattleboro, VT, USA) through a 510WB40 emission filter (Omega Optical, Brattleboro, VT, USA) onto a CoolSNAP HQ monochrome CCD camera (Roper Scientific, Vianen, The Netherlands). The integration time of the CCD camera was set at 200ms with a sampling interval of 3 seconds. After 30 seconds of measuring, either ATP (100 μM) in Ca-HT, ATP (100 μM) + MRS2500 (1 μM) in Ca-HT or just Ca-HT was added to the mini-well. At each timepoint the 340/380nm ratio was calculated per region. To determine the maximal response, the delta peak was calculated by subtracting the baseline ratio from the maximum ratio for every cell. Only the responding cells were used for data analysis.

2.8 | Immunocytochemistry

Primary cilia in mDCT15 cells were visualized as previously described.[42] The following antibodies were used: primary antibody rabbit polyclonal anti-ARL13B (1:200, Proteintech, Rosemont, IL, USA) and secondary antibody Alexa Fluor 594-conjugated anti-rabbit IgG (1:250, Molecular Probes, Eugene, OR, USA). Nuclei were counterstained and cells mounted using DAPI-Fluoromount-G (ITK Diagnostics, Uithoorn, The Netherlands). Acquisition of images was performed using confocal laser scanning microscopy (FV1000, Olympus, Tokyo, Japan) equipped with a 60X oil-immersion objective. ARL13B-positive primary cilia (594 nm laser), identified as dots or small dashes on the xy-plane, and DAPI-positive nuclei (405 nm laser) were visualized. A z-stack with 0.25 μM distance between each focal plane was obtained. Images were processed using Fiji (https://fiji.sc/) software (National Institutes of Health, Bethesda, MD, USA).

2.9 | sgRNA design

Guide RNA's (sgRNA) targeting exon 9 of the *Mus musculus* gene *Pkd1* and exon 1 of the *Mus musculus* gene *Panx1* were designed using http://crispor.tefor.net/ (Supporting Table S1).[43] The oligonucleotide pair for each sgRNA was phosphorylated and annealed using T4 Polynucleotide Kinase (New England Biolabs, Ipswich, MA, USA) in a thermocycler (37°C for 30 minutes, 95°C for 5 minutes and ramped down to 25°C with 5°C/min). The plasmids PX458 (Addgene #48138)[44] and PX333 (Addgene #64073)[45] were linearized using *BbsI, or BsaI,* restriction enzymes (New England Biolabs, Ipswich, MA, USA) at 37°C for 1hr. The annealed oligonucleotides were ligated into the linearized PX458 or PX333 plasmid using T4 Ligase (New England Biolabs, Ipswich, MA, USA) overnight at 16°C. Next, the ligation mix was transformed by 42°C heat shock into TOP10F competent cells. The next day, colonies were picked and the PX458 or PX333 plasmid, containing the sgRNA, isolated. The PX333 was modified by inserting *T2A-eGFP* (derived from PX458) after *NLS-Cas9-NLS* resulting in the plasmid PX333-GFP, suitable for GFP-positive FACS sorting. The PX333 plasmid allows for the dual expression of sgRNA's.

2.10 | CRISPR/Cas9-mediated genome editing

mDCT15 cells were transfected with the PX458 (Addgene #48138,[44] or PX333-GFP plasmid (modified from Addgene #64073),[45] containing the sgRNA's, using Lipofectamin 2000 reagent (Invitrogen, Carlsbad, CA, USA). GFP-positive cells were single cell sorted into 96-well plates by fluorescence-activated cell sorting (FACS, Aria, BD Biosciences, San Jose, CA, USA) at 48 hours post-transfection. Next, single cell clones were grown (37°C, 5% (v/v) CO_2) for 7 to 14days in DMEM/F-12 1:1 nutrient mixed media (Thermo Fisher Scientific, Waltham, MA, USA) supplemented with 5% (v/v) FBS (GE Healthcare, Little Chalfont, United Kingdom) and ciprofloxacin (10 μg/mL). Once cells reached confluency, genomic DNA was isolated using the prepGEM DNA extraction kit (ZyGEM, Hamilton, New Zealand). The targeted region of either *Ift140* exon 8 or *Pkd1* exon 9 was amplified using AmpliTaq GOLD (Thermo Fisher Scientific, Waltham, MA, USA) in a thermocycler (95°C for 5 min and 30 cycles of 95°C for 15 seconds, 58°C for 30 s, and 72°C for 30 s followed by a final elongation step of 72°C for 7 min). PCR products were run on a 2% (w/v) agarose gel to assess that one single amplicon was amplified for the PX458 transfected cells, as for the PX333-GFP transfected cells, multiple amplicons corresponding to wild type, hetero- or homozygous can be expected. Next, PCR products were ligated into the pGEM-T Easy vector (Promega, Madison, WI, USA) using TA cloning and transformed into TOP10F competent cells. Plasmids containing an insert were sequenced, using sanger sequencing and SnapGene software (version 4.2.4, GSL Biotech LLC, Chicago, IL, USA), to assess each clone for homozygous frame shift mutations. The $Pkd1^{-/-}$ mDCT15 clones were validated by western blot (Figure 5A) using 4%-15% Criterion TGX Precast Gels (Bio-Rad Laboratories, Hercules, CA, USA), PVDF membrane (Immobilon-P, Millipore Corporation, Bedford, MA, USA), and the antibodies mouse anti-PC1 (1:1000, Santa Cruz Biotechnology, Dallas, TX, USA) and peroxidase-conjugated sheep anti-mouse (1:10,000, Sigma-Aldrich, St. Louis, MO, USA). Blots were visualized using enhanced chemiluminescence (Thermo Fisher Scientific, Waltham, MA, USA). Both $Pkd1^{-/-}$ clones used in this study were generated independently by either use of the PX458 or PX333-GFP plasmid. The $Ift140^{-/-}$ mDCT15 cell line was

previously generated and validated by sanger sequencing and immunocytochemistry.[46]

2.11 | Zebrafish experimentation

The effect of BB-FCF on cyst growth was studied in an established zebrafish model of PKD, where PKD is induced by the use of a translation blocking morpholino (MO) targeting the zebrafish ortholog of human *PKD2* (*pkd2*).[47] Wild-type Tupfel long-fin zebrafish were used for experimentation. In brief, PKD was induced in zebrafish larvae by microinjecting one- to two-cell stage embryos with the following *pkd2*-MO:5′-AGGACGAACGCGACTGGAGCTCATC-3′. This MO has been previously validated as *pkd2*-morphants phenocopy *pkd2* mutants.[48] In parallel, control embryos were injected with a standard mismatch control MO (5′-CCTCTTACCTCAGTTACAATTTATA-3′), directed against a human β-globin intron mutation, at the amount of 2 ng/embryo (Gene Tools, Philomath, OR, USA). At 4 hours postfertilization (hpf), BB-FCF was added to the medium (standard E3 medium: 5mM NaCl, 0.17mM KCl, 0.33mM $CaCl_2$, 0.33mM $MgSO_4$) at a final concentration of 100 μM. Non-treated fish were also included in our study. In this case, only the vehicle (MilliQ water) was added (same volume as used when adding BB-FCF) to the medium. In total, four experimental groups were realized: two groups microinjected with the *pkd2*-MO, exposed and non-exposed to BB-FCF; and two groups microinjected with the mismatch control MO, exposed and non-exposed to BB-FCF. At 5days postfertilization (dpf) larvae were anesthetized with tricaine/Tris pH 7.0 solution. Using brightfield microscopy (20x magnification) mortality, pronephros cystic phenotype, curved tail and pericardial edema were assessed, and high-resolution images of larvae were obtained. Images were processed using Fiji (https://fiji.sc/) software (National Institutes of Health, Bethesda, MD, USA) (Supporting Figure S1*A,B*). All animal procedures detailed here were performed in accordance with national and international legislations and were approved by the ethical review committee of the Radboud University Nijmegen.

2.12 | Statistical analyses

Differences between groups were analyzed using an unpaired Student's t test when two experimental groups were compared and a factor of variance was considered. When more than two experimental groups were considered, a one-way (one factor of variance) or a two-way ANOVA (two factors of variance) was applied, followed by the Tukey's test for multiple comparisons. Data in the figures are expressed as mean ± SEM. In the case of the experiments performed in vitro, the mean is the average value of independent experiments (n = 3-4). Each independent experiment consisted of at least two (in the case of ATP measurements) or three (in the case of gene expression measurements) replicates for each of the conditions tested. For in vivo experiments, the sample size is depicted in the figure legend. Differences in survival of zebrafish larvae were analyzed with the logrank (Mantel-Cox) test. $P < .05$ was considered statistically significant. All statistical analyses were performed with Prism 8 (GraphPad, La Jolla, CA, USA).

3 | RESULTS

3.1 | Flow modulates ATP extrusion in vitro and in vivo

To assess whether FSS influences the cellular ATP release from renal cells, mDCT15 cells were exposed to physiological FSS (Figure 1A). Cell morphology and monolayer integrity were not affected by the culture conditions (Figure 1B). A significant elevated ATP release was observed in cells exposed to 1.2 dyn/cm^2 FSS for 1 minute when compared to 0.3 dyn/cm^2 FSS (100 ± 75 vs 481 ± 127%, $P < .05$) (Figure 1C). ATP release attenuated when cells were exposed up to 5 minutes to these rates (Figure 1D-F). Cells exposed to cycles of alternating 1 minute exposures to 0.3 and 1.2 dyn/cm^2 followed by 1 minute rest displayed episodic peaks of ATP release when switching from 0.3 to 1.2 dyn/cm^2 FSS (100 ± 31 vs 220 ± 23% and 5 ± 1 vs 19 ± 4%, respectively, $P < .05$). Increasing the static interval to 25 minutes resulted in higher ATP release after applying FSS compared to a static interval of 1 minute (7 ± 5 vs 69 ± 11%, $P < .05$) (Figure 1G). To assess whether ATP extrusion is FSS-modulated in vivo, an acute water loading test in healthy human subjects was performed. Acute water loading significantly increased the urinary output, indicative of elevated urinary flow, resulting in higher urinary ATP excretion (27 ± 12 vs 2,426 ± 530 and 27 ± 12 vs 2,951 ± 696 pmol ATP/mmol creatinine for $t = 0$ vs $t = 60$ and $t = 0$ vs $t = 90$ minutes, respectively, $P < .05$) (Figure 1H). Overtime, urinary output decreased, resulting in lower urinary ATP excretion (2,951 ± 696 vs 901 ± 266 pmol ATP/mmol creatinine for $t = 90$ vs $t = 150$ minutes, respectively, $P < .05$).

3.2 | ATP extrusion not dependent on primary cilia

Studies have shown that FSS-modulated ATP release is primary cilia-dependent.[49] Therefore, *Ift140*$^{-/-}$ mDCT15 cells were used, where ciliogenesis is inhibited, to study the ATP extrusion upon FSS mechanosensation.[46] After staining for

the primary cilia-specific protein ARL13B, no primary cilia were detected in *Ift140*$^{-/-}$ cells. Wild-type cells displayed primary cilia (Figure 2A). Cells exposed to 0.3 and 1.2 dyn/cm^2 FSS exhibited similar FSS-modulated ATP release between wild-type and *Ift140*$^{-/-}$ cells (100 ± 34 vs 894 ± 107 and 100 ± 44 vs 770 ± 274%, respectively, $P < .05$) (Figure 2B).

3.3 | mTORC1 inhibition amplifies flow-modulated ATP release

Because mTORC1 is inhibited in cells upon flow sensing, the role of mTORC1 in FSS-modulated ATP release was investigated.[50] In detail, mDCT15 cells pre-incubated with 100nM rapamycin for 1hr and untreated cells were exposed to either 0.3 or 1.2 dyn/cm^2 FSS. The FSS-modulated ATP release was significantly increased in rapamycin-treated cells as compared to untreated cells (963 ± 123 vs 147 ± 19 and 445 ± 60 vs 100 ± 34%, respectively, $P < .05$) (Figure 3A). Furthermore, the intracellular ATP levels in rapamycin-treated cells were significantly higher than untreated cells (144 ± 16 vs 100 ± 5 and 153 ± 7 vs 99 ± 7%, $P < .05$) (Figure 3B).

3.4 | Flow regulates *P2ry1*, *P2rx5*, *Entpd2,* and *Entpd3* expression

In order to investigate whether FSS affects the purinergic signaling in mDCT15 cells, wild-type cells were exposed to static fluid and 0.6 dyn/cm^2 FSS for 3 hours. A significant increase in *P2rx5* and *P2ry1* mRNA was observed after exposure to 0.6 dyn/cm^2 FSS when compared to static controls (267 ± 58 vs 101 ± 10 and 195 ± 26 vs 101 ± 10%, respectively, $P < .05$). No changes in mRNA expression of *P2rx4*, *P2rx6*, *P2rx7,* and *P2ry2* were observed (101 ± 9 vs 119 ± 5, $P = .16$; 100 ± 5 vs 119 ± 10, $P = .16$; 102 ± 12 vs 95 ± 17, $P = .77$; and 103 ± 18 vs 116 ± 15%, $P = .61$, respectively) (Supporting Figure S2*B-G*). Expression of FSS-sensitive gene *Ptgs2* (Cox-2) was measured as positive control indicating the mRNA expression under FSS (131 ± 69 vs 660 ± 220%, $P = .08$) (Supporting Figure S2*A*).[42] Significantly higher mRNA expression of *Entpd2* and *Entpd3* was detected after exposure to FSS, whereas the mRNA expression of *Nt5e* was not altered (105 ± 24 vs 533 ± 132%, $P < .05$, 105 ± 24 vs 503 ± 104%, $P < .05$ and 101 ± 9 vs 79 ± 10%, $P = .20$, respectively) (Supporting Figure S2*H-J*). Since extracellular ATP is known to affect intracellular Ca^{2+} levels via purinergic receptors, mDCT15 cells were exposed to 100 μM extracellular ATP. Consequently, increased intracellular Ca^{2+} was observed 10 seconds after the ATP exposure. This response was significantly attenuated when cells were incubated with 10 μM MRS2500, a specific P2Y1 inhibitor (0.79 ± 0.02 vs 0.59 ± 0.03ΔPeak, $P < .05$) (Supporting Figure S3).[51]

3.5 | Pannexin-1 contributes to flow-modulated ATP extrusion

In order to identify the extrusion mechanisms gating FSS-modulated ATP release, mRNA expression of candidates mediating the ATP release was assessed after mDCT15 cells were exposed to either static or 0.6 dyn/cm^2 FSS (Figure 4A). In virtue of their expression in kidney, pannexin-1, connexin-37,

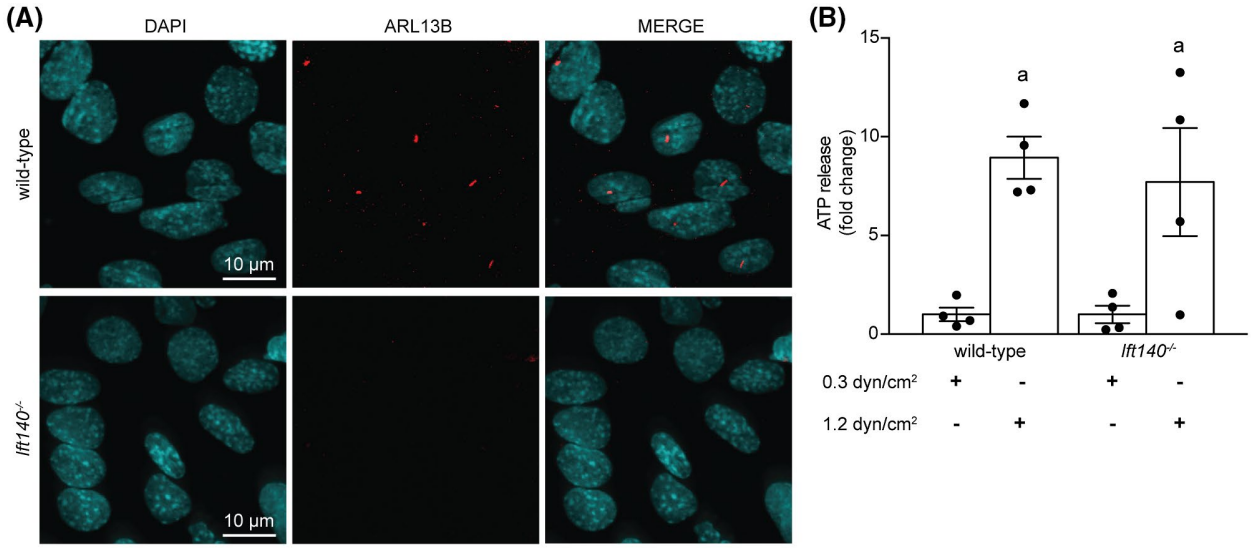

FIGURE 2 FSS-modulated ATP release is not dependent on the presence of primary cilia. A, Immunocytochemical observation of primary cilia, detected through ARL13B staining, in wild-type mDCT15 cells. In *Ift140*$^{-/-}$ mDCT15 cells no primary cilia were observed. B, Elevated ATP release in both wild-type and *Ift140*$^{-/-}$ mDCT15 cells exposed to 1 min of 1.2 dyn/cm^2 FSS as compared to 1 min of 0.3 dyn/cm^2 FSS (n = 4). Values are presented as the mean ± SEM, significant differences ($P < .05$) are denoted with symbol a

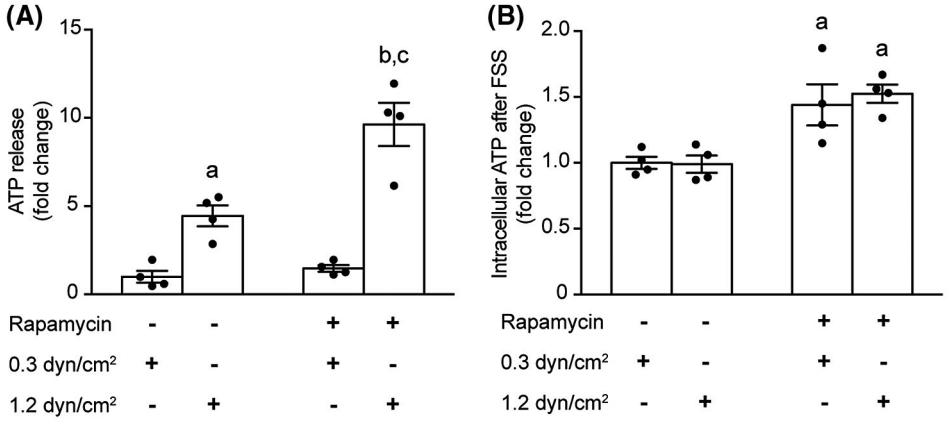

FIGURE 3 Inhibition of mTORC1 by rapamycin amplifies FSS-modulated ATP release and increases intracellular ATP. A, FSS-modulated ATP release of wild-type mDCT15 cells exposed for 1 min to either 0.3 or 1.2 dyn/cm^2 FSS and pre-incubated with or without 100 nM rapamycin. B, Intracellular ATP of wild-type mDCT15 cells exposed for 1 min to either 0.3 or 1.2 dyn/cm^2 FSS and pre-incubated with or without 100 nM rapamycin. Values are presented as the mean ± SEM (n = 4). Significant differences ($P < .05$) between 0.3 and 1.2 dyn/cm^2 FSS without rapamycin are denoted with symbol a, significant differences ($P < .05$) between 0.3 and 1.2 dyn/cm^2 FSS with rapamycin are denoted with symbol b, significant differences ($P < .05$) between 1.2 dyn/cm^2 FSS incubated with or without rapamycin are denoted with symbol c

and Abcc6 were considered to regulate FSS-sensitive ATP extrusion.[52-54] A significant increase in *Panx1* mRNA, but not *Cx37* and *Abcc6,* was observed in wild-type cells after exposure to 0.6 dyn/cm^2 FSS when compared to static (297 ± 28 vs 111 ± 37%, $P < .05$, 112 ± 8 vs 101 ± 8%, $P = .37$ and 100 ± 4 vs 107 ± 6%, $P = .42$, respectively) (Figure 4B-D). To further investigate whether pannexin-1 channels mediate the FSS-rate sensitive ATP release, wild-type and *Panx1*$^{-/-}$ mDCT15 cells were exposed to 0.3 and 1.2 dyn/cm^2 with or without 100 μM brilliant blue FCF (BB-FCF). Via sanger sequencing a homozygous deletion starting in 5′UTR and ending in exon 1 (g.15,045,106_15,044,905del) was observed in *Panx1*$^{-/-}$ cells, effectively removing the start codon for Pannexin-1 (Supporting Figure S4). An increased ATP release was observed when wild-type cells were subjected to 1.2 dyn/cm^2 compared to cells subjected to 0.3 dyn/cm^2 FSS (586 ± 143 vs 100 ± 25%, $P < .05$). With cells subjected to 1.2 dyn/cm^2 FSS, a significant decreased FSS-modulated ATP release was observed in wild-type cells exposed to BB-FCF when compared to non-exposed cells (586 ± 143 vs 231 ± 41%, $P < .05$). *Panx1*$^{-/-}$ cells, with or without BB-FCF, displayed a similar decreased FSS-modulated ATP release when compared to non-exposed wild-type cells (586 ± 143 vs 283 ± 24%, $P < .05$, 586 ± 143 vs 285 ± 80%, $P < .05$) (Figure 4E). These in vitro data illustrate pannexin-1 as an important extrusion mechanism for FSS-modulated ATP release in mDCT15 cells.

3.6 | Variable flow has no effect on ATP release when polycystin-1 function is lost

Since urinary ATP excretion is elevated in *iKsp-Pkd1*^{del} mice, experiments were designed to assess the role of PC1 in renal FSS-modulated ATP release. To this end, *Pkd1*$^{-/-}$ mDCT15 cells were generated and validated (Figure 5A). ARL13B-positive primary cilia were detected in *Pkd1*$^{-/-}$ cells (Figure 5B). ATP extrusion was observed when *Pkd1*$^{-/-}$ cells were exposed to 0.3 and 1.2 dyn/cm^2 FSS. Significantly higher ATP release after 0.3 dyn/cm^2 exposure in *Pkd1*$^{-/-}$ cells was observed vs wild-type cells (775 ± 250 vs 100 ± 34%, $P < .05$) (Figure 5C). When *Pkd1*$^{-/-}$ cells were exposed to 1.2 dyn/cm^2 FSS, similar increased ATP release was observed when compared to wild-type cells (526 ± 302 vs 100 ± 42%, $P = .13$) (Figure 5E). Intracellularly, ATP levels were significantly increased in *Pkd1*$^{-/-}$ vs wild-type cells (255 ± 56 vs 100 ± 5 and 211 ± 18 vs 100 ± 7%, $P < .05$) (Figure 5D,F). ATP release measured in *Pkd1*$^{-/-}$ mDCT15 cells was not sensitive to varying FSS. mTOR inhibition, using 100 nM rapamycin, did not amplify FSS-modulated ATP release in these cells (100 ± 52 vs 120 ± 65, $P = .99$ and 235 ± 113 vs 331 ± 150%, $P = .91$, respectively) (Figure 5G). In contrast with wild-type cells, treatment of *Pkd1*$^{-/-}$ cells with 100 nM rapamycin had no significant effect on intracellular ATP (100 ± 24 vs 96 ± 22, $P = .99$ and 92 ± 16 vs 100 ± 18%, $P = .99$, respectively) (Figure 5H). These data were reproduced in a second, independently generated, *Pkd1*$^{-/-}$ clone (Supporting Figure S5).

3.7 | Pannexin-1 mediates increased basal ATP extrusion when polycystin-1 is dysfunctional

There is growing evidence indicating extracellular ATP may contribute to PKD pathogenesis.[24] Therefore, we investigated the role of ATP in *Pkd1*$^{-/-}$ mDCT15 cells and *iKsp-Pkd1*^{del} mice. Wild-type and *Pkd1*$^{-/-}$ mDCT15 cells were exposed to

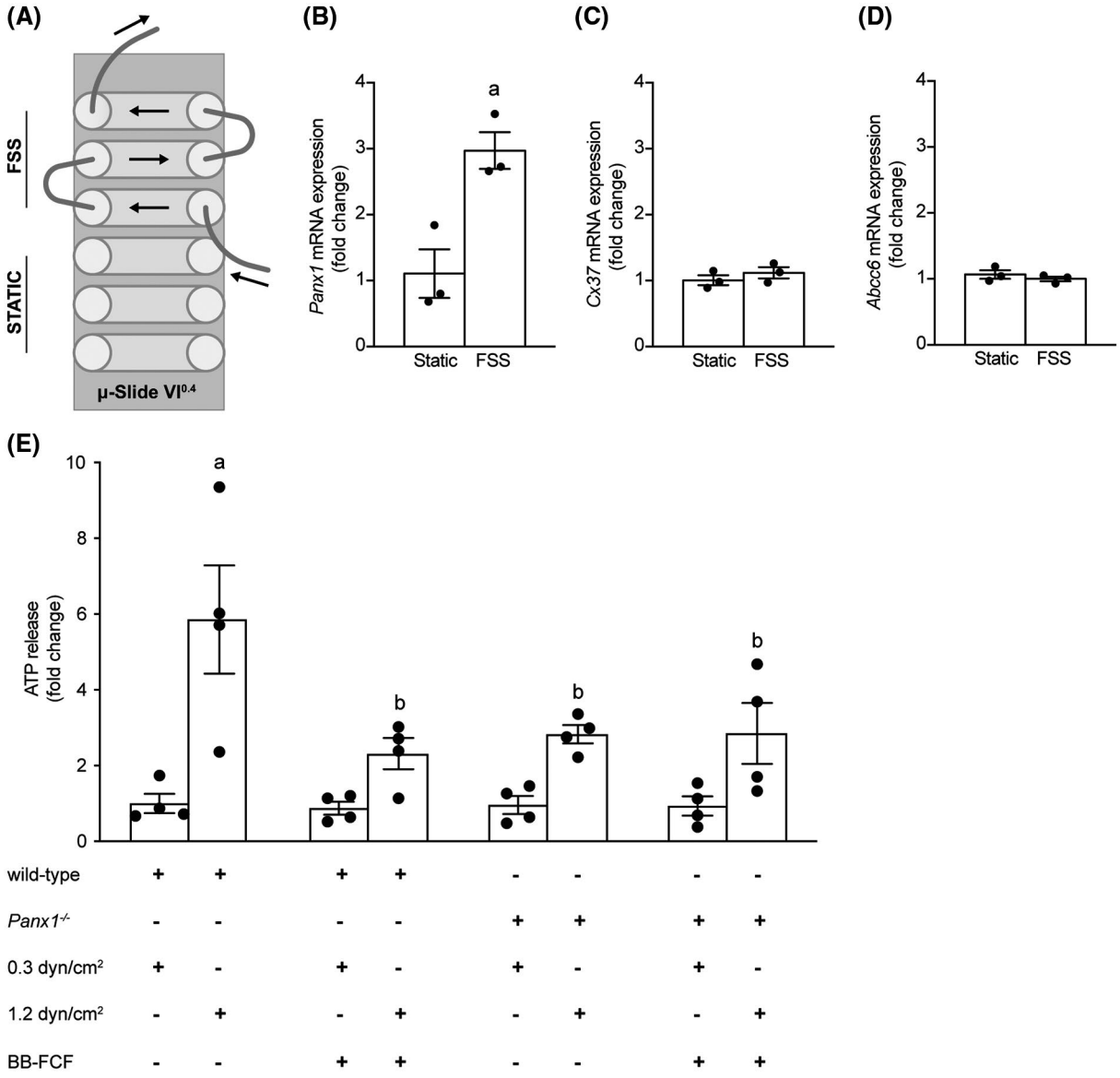

FIGURE 4 Pannexin-1 mediates FSS-modulated ATP release in vitro. A, Schematic overview of in vitro microfluidic set-up for all gene expression experiments performed in this study. B-D, mRNA expression of *Panx1*, *Cx37,* and *Abcc6* after 3 h of 0.6 dyn/cm^2 FSS as compared to static conditions (n = 3). E, FSS-modulated ATP release of wild-type and *Panx1*$^{-/-}$ mDCT15 cells exposed for 1 min to either 0.3 and 1.2 dyn/cm^2 FSS and incubated with or without 100 μM BB-FCF (n = 4). Values are presented as the mean ± SEM, significant differences ($P < .05$) are denoted with symbol a (ie, static to 0.6 dyn/cm^2 or 0.3 to 1.2 dyn/cm^2) or b (wild-type 1.2 dyn/cm^2 without BB-FCF to *Panx1*$^{-/-}$ 1.2 dyn/cm^2 without BB-FCF or wild-type and *Panx1*$^{-/-}$ 1.2 dyn/cm^2 with BB-FCF)

0.6 dyn/cm^2 FSS or a static environment. In line with elevated ATP release of *Pkd1*$^{-/-}$ cells, significantly increased *Panx1* mRNA was observed in *Pkd1*$^{-/-}$ vs wild-type cells under static conditions (776 ± 91 vs 101 ± 9%, $P < .05$) (Figure 6A). mRNA of *Cx37* and *Abcc6* were not altered (105 ± 21 vs 79 ± 18 and 100 ± 4 vs 128 ± 25%, respectively, $P > .05$) (Figure 6B-C). Similar results were obtained when cells were exposed to 0.6 dyn/cm^2 FSS (Supporting Figure S6). ATP release of *Pkd1*$^{-/-}$ cells exposed to 1.2 dyn/cm^2 FSS was reduced when incubated with 100 μM BB-FCF as compared to non-incubated cells (48 ± 14 vs 105 ± 28%, $P < .05$) (Figure 6D). Under static, ATP release was significantly increased in *Pkd1*$^{-/-}$ vs wild-type cells (202 ± 22 vs 100 ± 28%, $P < .05$). Incubation of *Pkd1*$^{-/-}$ cells with 100 μM BB-FCF inhibited ATP extrusion in static conditions (114 ± 15 vs 202 ± 22%, $P < .05$), whereas in wild-type cells no decrease in static ATP release was observed when exposed to 100 μM BB-FCF (79 ± 11 vs 100 ± 28%, $P = .87$) (Figure 6E). In line with the in vitro findings, a significant higher urinary ATP excretion was observed in *iKsp-Pkd1*^{del} mice compared to non-induced age and genotype-matched controls (2.05 ± 0.24 vs 0.81 ± 0.22 pmol/24 h, $P < .05$) (Figure 6F). Furthermore, *iKsp-Pkd1*^{del} mice showed increased renal *Panx1* mRNA compared to controls (141 ± 18 vs 100 ± 4%, $P < .05$) (Figure 6G).

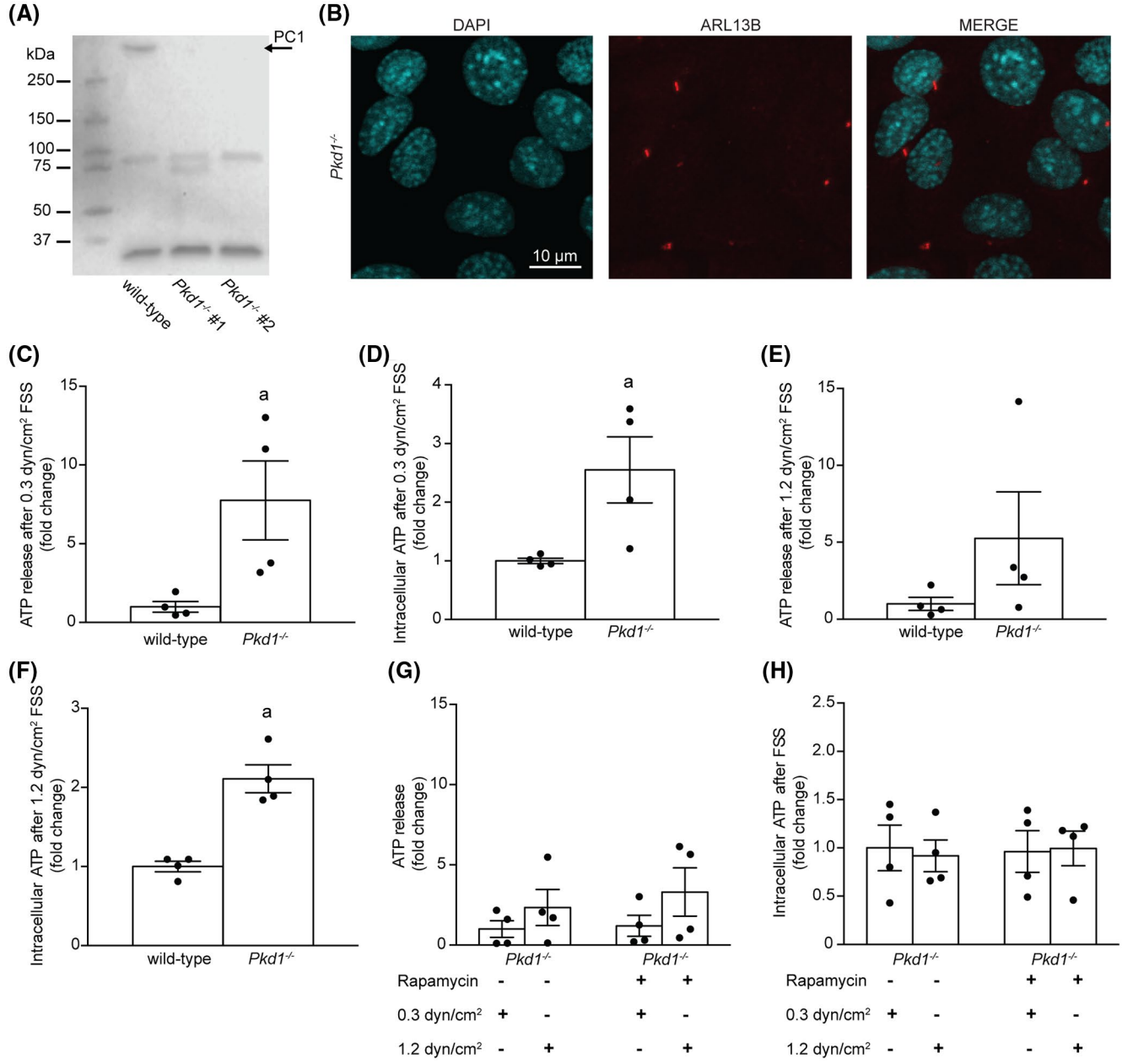

FIGURE 5 Loss of Polycystin-1 function lacks FSS-modulated ATP extrusion. A, Western blot validation (anti-Polycystin-1, 7E12) of CRISPR/Cas9 generated *Pkd1*$^{-/-}$ mDCT15 clones; clone 1 compound heterozygous for the mutations p.Arg605Leu*fs**16 and p.Gln607Leu*fs**16, clone 2 homozygous for the mutation p.Ser612Gly*fs**67. The second band in clone 1 corresponds to the expected truncated mutant PC1 protein size after DNA sequencing analysis. B, Immunocytochemistry observation of primary cilia, detected via staining for ARL13B, in *Pkd1*$^{-/-}$ mDCT15 cells. C and D, ATP release and intracellular ATP, respectively, of wild-type and *Pkd1*$^{-/-}$ mDCT15 cells exposed for 1 min to 0.3 dyn/cm^2 FSS. E and F, ATP release and intracellular ATP, respectively, of wild-type and *Pkd1*$^{-/-}$ mDCT15 cells exposed for 1 min to 1.2 dyn/cm^2 FSS. G and H, ATP release and intracellular ATP, respectively, of wild-type and *Pkd1*$^{-/-}$ mDCT15 cells exposed for 1 min to 0.3 or 1.2 dyn/cm^2 FSS with or without 100 nM rapamycin incubation. Values are presented as the mean ± SEM (n = 4), significant differences ($P < .05$) are denoted with symbol a

3.8 | Pannexin-1 inhibition attenuates cyst growth in a zebrafish model for PKD

Our data indicate that, in PKD, purinergic signaling is dysregulated with respect to the healthy context. Therefore, inhibition of ATP release through pannexin-1 could attenuate the disease progression. This hypothesis was tested in a zebrafish PKD model. Renal cyst formation, the hallmark of PKD, was observed in zebrafish after inhibition of the ortholog of human *PKD2*, *pkd2*, one of the genes mutated in PKD.[47] Typical *pkd2* morphant phenotype (cystic pronephros and curved tail) was observed in larvae injected with *pkd2*-MO at 5dpf, while control fish (injected with control MO) did not display any morphological abnormality (Figure 7A-C). Conspicuously,

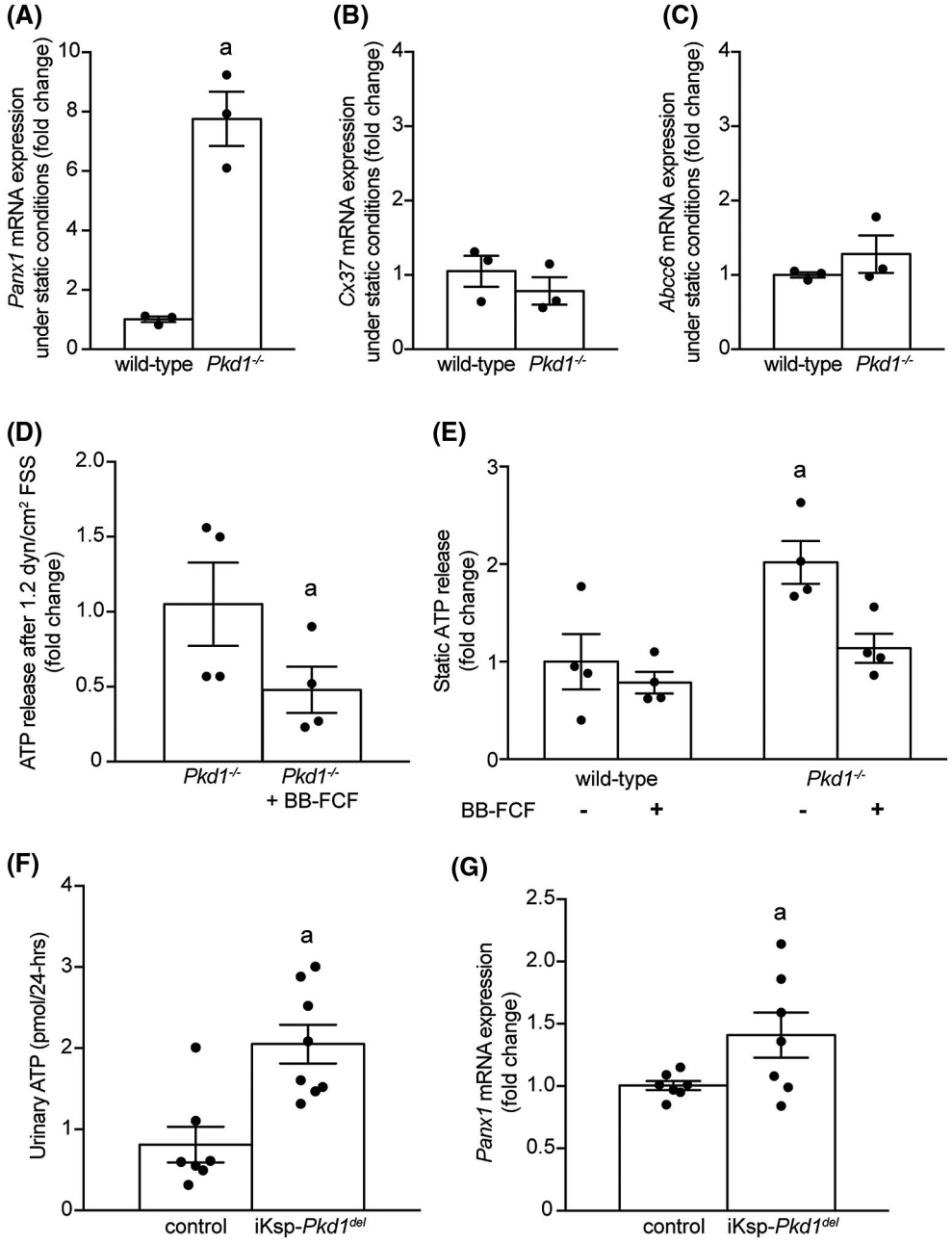

FIGURE 6 Pannexin-1 expression and ATP extrusion, in vitro and in vivo, is elevated when polycystin-1 is dysfunctional. A-C, mRNA expression of *Panx1*, *Cx37,* and *Abcc6* in $Pkd1^{-/-}$ mDCT15 cells as compared to wild-type mDCT15 cells after 3 h of 0.6 dyn/cm^2 FSS exposure (n = 3). D, ATP release of $Pkd1^{-/-}$ mDCT15 cells exposed for 1 min to 1.2 dyn/cm^2 FSS and incubated with or without 100 μM BB-FCF (n = 4). E, Static ATP release of wild-type mDCT15 and $Pkd1^{-/-}$ mDCT15 cells incubated with or without 100 μM BB-FCF (n = 4), in this panel symbol a indicates significant difference with wild type treated and untreated with BB-FCF, and $Pkd1^{-/-}$ treated with BB-FCF. F, Urinary ATP levels (pmol/24 h) of pre-cystic iKsp-$Pkd1^{del}$ and control mice (PN18 + 29days, n = 7-8). G, *Panx1* mRNA expression of pre-cystic iKsp-$Pkd1^{del}$ and control mice (PN18 + 29days, n = 7-8). Values are presented as the mean ± SEM, significant differences ($P < .05$) are denoted with symbol a

cyst growth in *pkd2* morphants was attenuated in morphants exposed to 100 μM BB-FCF from 4hpf to 5dpf (Figure 7D), a treatment with no effects on control fish morphology (Figure 7B). Additionally, in *pkd2* morphants treated with BB-FCF, increased survival was observed at 5dpf, compared to non-exposed *pkd2* morphants (82% and 24%, respectively) (Figure 7E). *pkd2* morphants exposed to BB-FCF displayed similar degree of cyst formation as untreated *pkd2* morphants (Figure 7F), but cysts were significantly smaller in BB-FCF-exposed *pkd2* morphants (319 ± 28 vs 119 ± 13%, $P < .05$) (Figure 7G). No changes in pericardial edema area or the number of curly tails, characteristic features of *pkd2* morphants,[47] were observed upon BB-FCF treatment (5 ± 1 vs 6 ± 1%, $P = .49$ for the pericardial edema area) (Figure 7H,I).

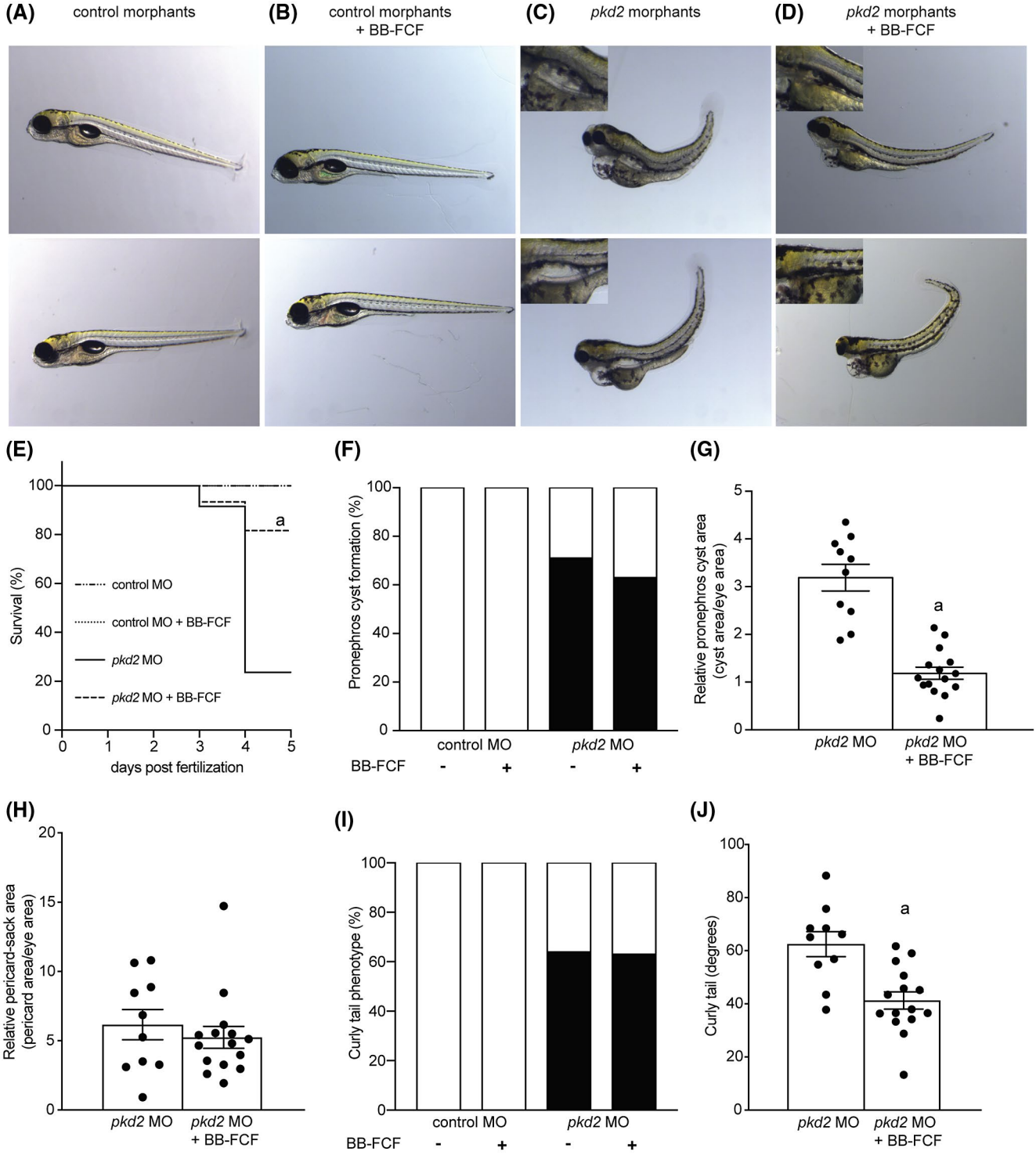

FIGURE 7 Inhibition of Pannexin-1 channels in a zebrafish PKD model results in decreased cyst growth. A and B, Phenotypic brightfield images of representative zebrafish larvae (5days postfertilization) after treatment with control MO (A) or with control MO plus 100 μM BB-FCF (B) (20x magnification). C and D, Phenotypic brightfield images of representative zebrafish larvae (5days postfertilization) after treatment with *pkd2* MO (C) or with *pkd2* MO plus 100 μM BB-FCF (D) (20x magnification). Zoomed-in image of pronephros cyst is depicted in image-box in left upper corner. (E) Survival percentage of zebrafish larvae (5days postfertilization) upon treatment with control MO, with (100% survival) or without (100% survival) 100 μM BB-FCF administration, or upon treatment with *pkd2* MO, with (82% survival) or without (24% survival) 100 μM BB-FCF. (F) Percentage of zebrafish larvae displaying a pronephros cyst after treatment of control MO with (n = 20) or without (n = 20) 100 μM BB-FCF administration and *pkd2* MO with (n = 24) or without 100 μM BB-FCF (n = 14). (G) Relative pronephros cyst area in zebrafish larvae (5 days postfertilization) after treatment of *pkd2* MO with (n = 15) or without (n = 10) 100 μM BB-FCF. (H) Pericard-sack area (pericardial edema) relative to the eye area of *pkd2* morphants (n = 10) and *pkd2* morphants treated with 100 μM BB-FCF (n = 15). (I) Percentage of zebrafish larvae displaying curled tail phenotype (black bars). (J) Degree of tail bending (curved tail) of *pkd2* morphants (n = 10) and *pkd2* morphants treated with 100 μM BB-FCF (n = 15). Values are presented as the mean ± SEM, significant differences ($P < .05$) are denoted with symbol a

However, degree of tail bending was significantly reduced in *pkd2* morphants treated with BB-FCF (41.3 ± 3.2 vs 62.5 ± 4.7°, $P < .05$) (Figure 7J).

4 | DISCUSSION

This study demonstrates that the renal ATP-channel pannexin-1 is key for release of ATP from tubular epithelial cells toward the urinary compartment upon flow mechanosensation in physiological conditions and disease models of PKD. Moreover, our data show that inhibition of pannexin-1 attenuates the renal cyst growth, pointing to involvement of ATP excretion in PKD progression. These conclusions are substantiated by the following findings: *i*) *Panx1* expression is upregulated upon flow exposure in renal cells, and correlates with apical ATP release that is reduced when these cells are exposed to the specific pannexin-1 inhibitor BB-FCF; *ii*) *Panx1* expression and urinary ATP levels are higher in iKsp-*Pkd1*^{del} vs control mice, correlating with increased ATP extrusion and *Panx1* expression in *Pkd1*$^{-/-}$ *vs* wild-type cells; *iii*) cyst growth is attenuated in a zebrafish model of PKD (*pkd2* morphants) exposed to pannexin-1 inhibitor BB-FCF.

Tubular flow stimulates the ATP excretion by mDCT15 cells. Importantly, the FSS magnitudes employed in our study (0.3 to 1.2 dyn/cm^2) cover the expected physiological FSS for the nephron.[55-58] We aimed to translate this in vitro phenomenon to the in vivo situation. In this sense, urinary ATP excretion was higher with increased urinary output, as showed by the acute water loading test performed in human healthy subjects. Conversely, when urinary output decreases, urinary ATP excretion was also reduced. In turn, variations in extracellular ATP will have effect on purinergic signaling.[59] Purinergic ligands, including ATP, will interact with P2X/P2Y or P1 receptors, affecting kidney function, among others maintenance of electrolyte homeostasis.[16,34,60] In line with this, our findings indicate FSS-dependent expression of several purinergic components such as *P2ry1*, *P2rx5*, *Entpd2* and *Entpd3*. Exposing mDCT15 cells to extracellular ATP elicited an intracellular Ca^{2+} response, indicating that these cells are purinergically active. Furthermore, mDCT15 cells are a relevant model to use in this study since the cyst formation in PKD originates mainly from CD but also the distal tubule, including the thick ascending limb of Henle's loop and DCT.[1-4] In addition, ATP released from DCT can have a profound effect, via purinergic signaling, on the CD.

A link between FSS-modulated ATP release and primary cilia was not observed in the mDCT15 cells used in this study. Previously, flow-stimulated ATP release has been shown to be primary cilia-dependent.[33,49] However, primary cilia-independent ATP release has also been reported.[61] These discrepancies may be attributed to differences in the mechanical stimulation by flow such as the presence or absence of a variable pressure on the cell surface.[49] Our findings showed that FSS-modulated ATP release can occur without primary cilia, at least in mDCT15 cells.[36]

While FSS-modulated ATP release has effects on purinergic signaling and therefore on renal function, little is known about the molecular mechanism that regulates FSS-modulated ATP release. A link between mTORC1 and FSS was previously established in MDCK cells, in which primary cilia sensing of flow was implicated.[50] Interestingly, when rapamycin-incubated mDCT15 cells were exposed to 0.3 or 1.2 dyn/cm^2 FSS, cellular ATP release was amplified. This finding suggests a regulatory role of mTORC1 in FSS-modulated ATP release. In addition, we observed an FSS-insensitive increase in intracellular ATP levels by rapamycin. This observation might be attributed to the stimulation of glycolysis by rapamycin, as previously observed in other cell models.[62-64] We also observed an increase in intracellular ATP in *Pkd1*$^{-/-}$ cells compared to wild type. These observations are in line with a previous publication demonstrating enhanced glycolysis and increased intracellular ATP levels in *Pkd1*$^{-/-}$ cells and cystic kidney.[65] In this regard, the absence of a further increase in intracellular ATP in *Pkd1*$^{-/-}$ cells exposed to rapamycin might be attributed to a saturated glycolytic capacity or a negative regulation mechanism absent in wild-type cells.

Among the plethora of cellular ATP extrusion mechanisms, pannexin-1, connexin- 30 (Cx30), connexin-30.3 (Cx30.3), and connexin-37 (Cx37) can potentially mediate the urinary ATP excretion.[32,52,53] Pannexins and connexins form transmembrane channels with strong apical expression in renal tubular epithelial cells.[52,66] Previous studies showed that perfusion of tubules expressing Cx30, causes ATP release into the tubular lumen.[67,68] Renal Cx30 expression is restricted to the connecting tubule and CD.[53,69] In contrast, pannexin-1 and Cx37 are expressed ubiquitously along the nephron, whereas Cx30.3 is confined to CD.[52,53] Abcc6 mediates ATP release in liver and is expressed in kidney.[54,70] In our study, only the expression of *Panx1* was significantly increased when cells were exposed to 0.6 dyn/cm^2. Though the duration of FSS exposure was different between gene expression and ATP experiments, these findings suggest that pannexin-1 could be the primary regulator of FSS-modulated ATP extrusion. Indeed, inhibition and knockout of pannexin-1 reduced FSS-modulated ATP release.

PC1 and PC2, have been postulated to play a key role in mechanosensation.[12,71] We show that in a PKD mouse model, urinary ATP levels were increased compared to control mice, which has never been reported before.[15] Interestingly, *Panx1* expression levels were higher in iKsp-*Pkd1*^{del} vs control mice and these results were confirmed in *Pkd1*$^{-/-}$ cells. The increase in basal ATP release observed in *Pkd1*$^{-/-}$ cells was largely mediated via pannexin-1 since the pannexin-1 inhibitor BB-FCF significantly reduced this response. Importantly,

FSS did not enhance the ATP release in *Pkd1*$^{-/-}$ cells, corroborating the lack of mechanosensitive ATP extrusion in these cells. Dysfunctional PC1 also critically affects the transcriptome of kidney cells.[72] In addition, increased expression of pannexin-1 in cyst lining cells of a mouse and rat PKD model has recently been reported.[20,73] Under given stimuli (eg, mechanic stimulation, intracellular concentrations of certain ions, etc), higher pannexin-1 expression may result in higher transport activity. Our findings suggest that higher urinary ATP levels in PKD could be explained by an upregulation of *Panx1* expression, a feature that may be related to the PKD transcriptome.

Our findings are also in line with other studies showing elevated ATP release in primary PKD cells.[14,22] Furthermore, mTORC1 inhibition in *Pkd1*$^{-/-}$ cells did not enhance FSS-modulated ATP release, suggesting that PC1 is required for mTORC1 to regulate FSS-modulated ATP release. Conspicuously, intracellular ATP was higher in *Pkd1*$^{-/-}$ cells, however inhibition of mTORC1 did not increase intracellular ATP. These findings indicate that without PC1, ATP dynamics, both intra- and extracellular, are altered.

Elevated extracellular ATP levels are likely independent of flow sensing in PKD. This is highlighted by our in vivo and in vitro PKD models (iKsp-*Pkd1*^{del} mice and *Pkd1*$^{-/-}$ mDCT15 cells, respectively) where increased ATP extrusion was observed. In early PKD, hyperfiltration is common.[74] However, based on data displayed in the present study, this would not cause elevated ATP release since PC1 is required for FSS-modulated ATP extrusion. Strikingly, basal ATP extrusion is increased in *Pkd1*$^{-/-}$ cells and supported by elevated urinary ATP excretion in iKsp-*Pkd1*^{del} mice. The elevated extracellular ATP can be detrimental to PKD progression.[75] This is indicated by studies showing elevated expression of P2Y2, P2Y6 and P2X7 in a rat model of PKD, and that expression of both P2X4 and P2X7 increases during progression of PKD.[18,21] In addition, inhibition of P2X7 in a zebrafish PKD model reduced cyst formation.[76] Extracellular ATP has been shown to mediate chloride (Cl^-) secretion through Ca^{2+} signaling.[14] It is hypothesized that an elevated Cl^- secretion contributes to cyst growth. In fact, it was shown that activation of Cl^- channel TMEM16A, via P2Y2, promotes renal cyst growth.[77-79] In PKD, increased extracellular ATP may be available via pannexin-1, but also the expression profile of purinergic receptors is shifted in cystic epithelia toward increased P2X4 and P2X7 prevalence, enlarging detrimental effects of ATP on disease progression. Reducing extracellular ATP content as therapeutic approach for PKD could prove to be an interesting endeavor. Based on our findings with the zebrafish PKD model, pannexin-1 emerges as novel target to prevent cyst growth in PKD. Unlike probenecid, which is a well-known pannexin-1[20] but also P2X7 inhibitor,[80] the inhibitor used here, BB-FCF, has been demonstrated to be specific for pannexin-1 and does not target P2X7.[38] Thus, our findings unequivocally indicate the contribution of pannexin-1 to cyst growth and suggest this channel as druggable target for PKD therapy. Interestingly, pannexin-1 expression levels appear to be dramatically increased in pathological conditions compared to the healthy kidney making it an especially interesting therapeutic target.[73,81] BB-FCF, is considered safe to use. To be effective in humans, a higher daily dose of BB-FCF should be administered than the acceptable daily intake of 6mg/kg body weight/day set by the European

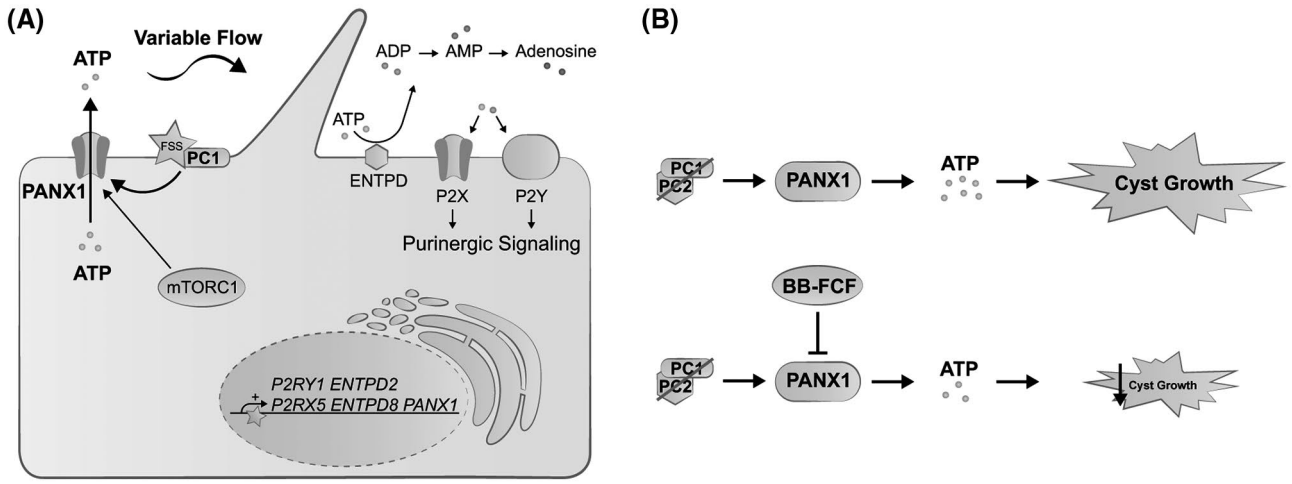

FIGURE 8 Polycystin-1 regulates pannexin-1 mediated purinergic signaling. (A) Variable pro-urinary flow is sensed and translated into a molecular signaling cascade involving the inhibition of mTORC1, increased function of PC1 and in turn activation or upregulation of pannexin-1 channels to release more ATP into the extracellular lumen. The extracellular ATP, and its hydrolysis products ADP, AMP, and adenosine, will evoke an activation of purinergic signaling. Long-term exposure to increased FSS results in the increased expression of various purinergic signaling components; that is, P2Y/P2X receptors and ectonucleotidases (ENTPDs). (B) In the case of PC1/PC2 loss-of-function, ATP release via pannexin-1 is increased followed by an augmented cyst growth. Inhibition of pannexin-1 channels (ie, using BB-FCF) decreases the elevated ATP release and reduces subsequent cyst growth when PC1/PC2 function is impaired

Food and Safety Authority.[82] A potential side effect using BB-FCF may be blue skin coloration.[38] Therefore, identifying structurally related compounds or other pannexin-1 inhibitors is warranted.

In summary, we present a novel mechanism for renal FSS-modulated ATP release through pannexin-1 channels regulated via PC1 (Figure 8). Our study strengthens the notion that extracellular ATP plays a key role in disease progression of PKD. Furthermore, our data suggest that inhibition of ATP release in PKD could reduce cyst growth. Thus, pannexin-1 is presented as novel therapeutic target in PKD.

ACKNOWLEDGMENTS

We thank Dr Omar AZ Tutakhel, Charlotte Roosendaal, Marieke Schultink, and Milou Fransen for their support and acknowledge Dr Erwin van Wijk and Dr Gert Flik for providing the facilities for zebrafish experimentation. This study is supported by grants from the Dutch Kidney Foundation (15OP03) to DJM Peters and RJM Bindels, and from the Netherlands Organization for Scientific Research (NWO VICI 016.130.668) to JGJ Hoenderop. JP Rigalli is supported by the Radboud Excellence Initiative from the Radboud University (Nijmegen, The Netherlands).

CONFLICT OF INTEREST

The authors declare that they have no conflicts of interests.

AUTHOR CONTRIBUTIONS

EV, JR, RB, DP, FA, and JH designed research; EV, JR, CM, MR, and FA performed research; EV, CM, and MR contributed new reagents or analytic tools; EV, JR, CM, MR, RB, DP, FA, and JH analyzed data; and EV, JR, RB, DP, FA, and JH wrote the paper. All authors read and approved the final manuscript.

REFERENCES

1. Bergmann C, Guay-Woodford LM, Harris PC, Horie S, Peters DJM, Torres VE. Polycystic kidney disease. *Nat Rev Dis Primers*. 2018;4:50.
2. Bergmann C. ARPKD and early manifestations of ADPKD: the original polycystic kidney disease and phenocopies. *Pediatr Nephrol*. 2015;30:15-30.
3. Happé H, van der Wal AM, Salvatori DCF, et al. Cyst expansion and regression in a mouse model of polycystic kidney disease. *Kidney Int*. 2013;83:1099-1108.
4. Shibazaki S, Yu Z, Nishio S, et al. Cyst formation and activation of the extracellular regulated kinase pathway after kidney specific inactivation of Pkd1. *Hum Mol Genet*. 2008;17:1505-1516.
5. Happé H, Peters DJM. Translational research in ADPKD: lessons from animal models. *Nat Rev Nephrol*. 2014;10:587-601.
6. Ong ACM, Devuyst O, Knebelmann B, Walz G, ERA-EDTA Working Group for Inherited Kidney Diseases. Autosomal dominant polycystic kidney disease: the changing face of clinical management. *Lancet*. 2015;385:1993-2002.
7. Xu GM, González-Perrett S, Essafi M, et al. Polycystin-1 activates and stabilizes the polycystin-2 channel. *J Biol Chem*. 2003;278:1457-1462.
8. Peters DJ, van de Wal A, Spruit L, et al. Cellular localization and tissue distribution of polycystin-1. *J Pathol*. 1999;188:439-446.
9. Markowitz GS, Cai Y, Li L, et al. Polycystin-2 expression is developmentally regulated. *Am J Physiol*. 1999;277:F17-F25.
10. Ward CJ, Turley H, Ong AC, et al. Polycystin, the polycystic kidney disease 1 protein, is expressed by epithelial cells in fetal, adult, and polycystic kidney. *Proc Natl Acad Sci U S A*. 1996;93:1524-1528.
11. Gilder AL, Chapin HC, Padovano V, Hueschen CL, Rajendran V, Caplan MJ. Newly synthesized polycystin-1 takes different trafficking pathways to the apical and ciliary membranes. *Traffic*. 2018;19:933-945.
12. Nauli SM, Alenghat FJ, Luo Y, et al. Polycystins 1 and 2 mediate mechanosensation in the primary cilium of kidney cells. *Nat Genet*. 2003;33:129-137.
13. Low SH, Vasanth S, Larson CH, et al. Polycystin-1, STAT6, and P100 function in a pathway that transduces ciliary mechanosensation and is activated in polycystic kidney disease. *Dev Cell*. 2006;10:57-69.
14. Schwiebert EM, Wallace DP, Braunstein GM, et al. Autocrine extracellular purinergic signaling in epithelial cells derived from polycystic kidneys. *Am J Physiol Renal Physiol*. 2002;282:F763-F775.
15. Rangan G. Role of extracellular ATP and P2 receptor signaling in regulating renal cyst growth and interstitial inflammation in polycystic kidney disease. *Front Physiol*. 2013;4:218.
16. Burnstock G, Evans LC, Bailey MA. Purinergic signalling in the kidney in health and disease. *Purinergic Signal*. 2014;10:71-101.
17. Hovater MB, Olteanu D, Welty EA, Schwiebert EM. Purinergic signaling in the lumen of a normal nephron and in remodeled PKD encapsulated cysts. *Purinergic Signal*. 2008;4:109-124.
18. Turner CM, Ramesh B, Srai SKS, Burnstock G, Unwin RJ. Altered ATP-sensitive P2 receptor subtype expression in the Han:SPRD cy/+ rat, a model of autosomal dominant polycystic kidney disease. *Cells Tissues Organs*. 2004;178:168-179.
19. Wildman SS, Hooper KM, Turner CM, et al. The isolated polycystin-1 cytoplasmic COOH terminus prolongs ATP-stimulated Cl^- conductance through increased Ca2+ entry. *Am J Physiol Renal Physiol*. 2003;285:F1168-F1178.
20. Arkhipov SN, Pavlov TS. ATP release into ADPKD cysts via pannexin-1/P2X7 channels decreases ENaC activity. *Biochem Biophys Res Commun*. 2019;513:166-171.
21. Palygin O, Ilatovskaya DV, Levchenko V, et al. Characterization of purinergic receptor expression in ARPKD cystic epithelia. *Purinergic Signal*. 2018;14:485-497.
22. Wilson PD, Hovater JS, Casey CC, Fortenberry JA, Schwiebert EM. ATP release mechanisms in primary cultures of epithelia derived from the cysts of polycystic kidneys. *J Am Soc Nephrol*. 1999;10:218-229.
23. Xu C, Shmukler BE, Nishimura K, et al. Attenuated, flow-induced ATP release contributes to absence of flow-sensitive, purinergic Cai2+ signaling in human ADPKD cyst epithelial cells. *Am J Physiol Renal Physiol*. 2009;296:F1464-F1476.
24. Ilatovskaya DV, Palygin O, Staruschenko A. Functional and therapeutic importance of purinergic signaling in polycystic kidney disease. *Am J Physiol Renal Physiol*. 2016;311:F1135-F1139.

25. Meijer E, Visser FW, van Aerts RMM, et al. Effect of lanreotide on kidney function in patients with autosomal dominant polycystic kidney disease: The DIPAK 1 randomized clinical trial. *JAMA*. 2018;320:2010-2019.
26. Shillingford JM, Murcia NS, Larson CH, et al. The mTOR pathway is regulated by polycystin-1, and its inhibition reverses renal cystogenesis in polycystic kidney disease. *Proc Natl Acad Sci U S A*. 2006;103:5466-5471.
27. Perico N, Antiga L, Caroli A, et al. Sirolimus therapy to halt the progression of ADPKD. *J Am Soc Nephrol*. 2010;21:1031-1040.
28. Edwards ME, Chebib FT, Irazabal MV, et al. Long-term administration of tolvaptan in autosomal dominant polycystic kidney disease. *Clin J Am Soc Nephrol*. 2018;13:1153-1161.
29. Torres VE, Chapman AB, Devuyst O, et al. Tolvaptan in later-stage autosomal dominant polycystic kidney disease. *N Engl J Med*. 2017;377:1930-1942.
30. Praetorius HA, Leipziger J. Fluid flow sensing and triggered nucleotide release in epithelia. *J Physiol*. 2008;586:2669-2669.
31. Jensen MEJ, Odgaard E, Christensen MH, Praetorius HA, Leipziger J. Flow-induced [Ca2+]i increase depends on nucleotide release and subsequent purinergic signaling in the intact nephron. *J Am Soc Nephrol*. 2007;18:2062-2070.
32. Praetorius HA, Leipziger J. ATP release from non-excitable cells. *Purinergic Signal*. 2009;5:433-446.
33. Hovater MB, Olteanu D, Hanson EL, et al. Loss of apical monocilia on collecting duct principal cells impairs ATP secretion across the apical cell surface and ATP-dependent and flow-induced calcium signals. *Purinergic Signal*. 2008;4:155-170.
34. Leipziger J. Control of epithelial transport via luminal P2 receptors. *Am J Physiol Renal Physiol*. 2003;284:F419-F432.
35. Solini A, Usuelli V, Fiorina P. The dark side of extracellular ATP in kidney diseases. *J Am Soc Nephrol*. 2015;26:1007-1016.
36. Ko B, Mistry AC, Hanson L, et al. A new model of the distal convoluted tubule. *Am J Physiol Renal Physiol*. 2012;303:F700-F710.
37. Ballou LM, Lin RZ. Rapamycin and mTOR kinase inhibitors. *J Chem Biol*. 2008;1:27-36.
38. Wang J, Jackson DG, Dahl G. The food dye FD&C Blue No. 1 is a selective inhibitor of the ATP release channel Panx1. *J Gen Physiol*. 2013;141:649-656.
39. Waikar SS, Sabbisetti VS, Bonventre JV. Normalization of urinary biomarkers to creatinine during changes in glomerular filtration rate. *Kidney Int*. 2010;78:486-494.
40. Tutakhel OAZ, Jeleń S, Valdez-Flores M, et al. Alternative splice variant of the thiazide-sensitive NaCl cotransporter: a novel player in renal salt handling. *Am J Physiol Renal Physiol*. 2016;310:F204-F216.
41. Verschuren EHJ, Mohammed SG, Leonhard WN, et al. Polycystin-1 dysfunction impairs electrolyte and water handling in a renal precystic mouse model for ADPKD. *Am J Physiol Renal Physiol*. 2018;315:F537-F546.
42. Mohammed SG, Arjona FJ, Verschuren EHJ, et al. Primary cilia–regulated transcriptome in the renal collecting duct. *FASEB J*. 2018;32:3653-3668.
43. Haeussler M, Schönig K, Eckert H, et al. Evaluation of off-target and on-target scoring algorithms and integration into the guide RNA selection tool CRISPOR. *Genome Biol*. 2016;17:707.
44. Ran FA, Hsu PD, Wright J, Agarwala V, Scott DA, Zhang F. Genome engineering using the CRISPR-Cas9 system. *Nat Protoc*. 2013;8:2281-2308.
45. Maddalo D, Manchado E, Concepcion CP, et al. In vivo engineering of oncogenic chromosomal rearrangements with the CRISPR/Cas9 system. *Nature*. 2014;516:423-427.
46. Verschuren EHJ, Hoenderop JGJ, Peters DJM, Arjona FJ, Bindels RJM. Tubular flow activates magnesium transport in the distal convoluted tubule. *FASEB J*. 2019;33:5034-5044.
47. Cao Y, Semanchik N, Lee SH, et al. Chemical modifier screen identifies HDAC inhibitors as suppressors of PKD models. *Proc Natl Acad Sci U S A*. 2009;106:21819-21824.
48. Sun Z, Amsterdam A, Pazour GJ, Cole DG, Miller MS, Hopkins N. A genetic screen in zebrafish identifies cilia genes as a principal cause of cystic kidney. *Development*. 2004;131:4085-4093.
49. Praetorius HA, Leipziger J. Released nucleotides amplify the cilium-dependent, flow-induced [Ca 2+] iresponse in MDCK cells. *Acta Physiologica*. 2009;197:241-251.
50. Boehlke C, Kotsis F, Patel V, et al. Primary cilia regulate mTORC1 activity and cell size through Lkb1. *Nat Cell Biol*. 2010;12:1115-1122.
51. Hechler B, Nonne C, Roh EJ, et al. MRS2500 [2-iodo-N6-methyl-(N)-methanocarba-2′-deoxyadenosine-3′,5′-bisphosphate], a potent, selective, and stable antagonist of the platelet P2Y1 receptor with strong antithrombotic activity in mice. *J Pharmacol Exp Ther*. 2006;316:556-563.
52. Hanner F, Lam L, Nguyen MTX, Yu A, Peti-Peterdi J. Intrarenal localization of the plasma membrane ATP channel pannexin1. *Am J Physiol Renal Physiol*. 2012;303:F1454-F1459.
53. Hanner F, Sorensen CM, Holstein-Rathlou N-H, Peti-Peterdi J. Connexins and the kidney. *Am J Physiol Regul Integr Comp Physiol*. 2010;298:R1143-R1155.
54. Jansen RS, Duijst S, Mahakena S, et al. ABCC6-mediated ATP secretion by the liver is the main source of the mineralization inhibitor inorganic pyrophosphate in the systemic circulation-brief report. *Arterioscler Thromb Vasc Biol*. 2014;34:1985-1989.
55. Weinbaum S, Duan Y, Thi MM, You L. An integrative review of mechanotransduction in endothelial, epithelial (renal) and dendritic cells (osteocytes). *Cell Mol Bioeng*. 2011;4:510-537.
56. Weinbaum S, Duan Y, Satlin LM, Wang T, Weinstein AM. Mechanotransduction in the renal tubule. *Am J Physiol Renal Physiol*. 2010;299:F1220-F1236.
57. Jang K-J, Suh K-Y. A multi-layer microfluidic device for efficient culture and analysis of renal tubular cells. *Lab Chip*. 2010;10:36-42.
58. Jang K-J, Cho HS, Kang DH, Bae WG, Kwon T-H, Suh K-Y. Fluid-shear-stress-induced translocation of aquaporin-2 and reorganization of actin cytoskeleton in renal tubular epithelial cells. *Integr Biol (Camb)*. 2011;3:134-141.
59. Shirley DG, Vekaria RM, Sévigny J. Ectonucleotidases in the kidney. *Purinergic Signal*. 2009;5:501-511.
60. Praetorius HA, Leipziger J. Intrarenal purinergic signaling in the control of renal tubular transport. *Annu Rev Physiol*. 2010;72:377-393.
61. Rodat-Despoix L, Hao J, Dandonneau M, Delmas P. Shear stress-induced Ca2+ mobilization in MDCK cells is ATP dependent, no matter the primary cilium. *Cell Calcium*. 2013;53:327-337.
62. Ramanathan A, Schreiber SL. Direct control of mitochondrial function by mTOR. *Proc Natl Acad Sci U S A*. 2009;106:22229-22232.
63. Chin TY, Kao CH, Wang HY, Huang WP, Ma KH, Chueh SH. Inhibition of the mammalian target of rapamycin promotes cyclic AMP-induced differentiation of NGO108-15 cells. *Autophagy*. 2010;6:1139-1156.

64. Zheng X, Boyer L, Jin M, et al. Alleviation of neuronal energy deficiency by mTOR inhibition as a treatment for mitochondria-related neurodegeneration. *Elife*. 2016;5:e13378.
65. Rowe I, Chiaravalli M, Mannella V, et al. Defective glucose metabolism in polycystic kidney disease identifies a new therapeutic strategy. *Nat Med*. 2013;19:488-493.
66. Stoessel A, Himmerkus N, Bleich M, Bachmann S, Theilig F. Connexin 37 is localized in renal epithelia and responds to changes in dietary salt intake. *Am J Physiol Renal Physiol*. 2010;298:F216-F223.
67. Sipos A, Vargas SL, Toma I, Hanner F, Willecke K, Peti-Peterdi J. Connexin 30 deficiency impairs renal tubular ATP release and pressure natriuresis. *J Am Soc Nephrol*. 2009;20:1724-1732.
68. Svenningsen P, Burford JL, Peti-Peterdi J. ATP releasing connexin 30 hemichannels mediate flow-induced calcium signaling in the collecting duct. *Front Physiol*. 2013;4:292.
69. Abed AB, Kavvadas P, Chadjichristos CE. Functional roles of connexins and pannexins in the kidney. *Cell Mol Life Sci*. 2015;72:2869-2877.
70. Matsuzaki Y, Nakano A, Jiang Q-J, Pulkkinen L, Uitto J. Tissue-specific expression of the ABCC6 gene. *J Invest Dermatol*. 2005;125:900-905.
71. Dalagiorgou G, Basdra EK, Papavassiliou AG. Polycystin-1: function as a mechanosensor. *Int J Biochem Cell Biol*. 2010;42:1610-1613.
72. Kunnen SJ, Malas TB, Formica C, Leonhard WN, 't Hoen PAC, Peters DJM. Comparative transcriptomics of shear stress treated Pkd1-/- cells and pre-cystic kidneys reveals pathways involved in early polycystic kidney disease. *Biomed Pharmacother*. 2018;108:1123-1134.
73. Arkhipov SN, Potter DL, Geurts AM, Pavlov TS. Knockout of P2rx7 purinergic receptor attenuates cyst growth in a rat model of ARPKD. *Am J Physiol Renal Physiol*. 2019;317:F1649-F1655.
74. Helal I, Reed B, McFann K, et al. Glomerular hyperfiltration and renal progression in children with autosomal dominant polycystic kidney disease. *Clin J Am Soc Nephrol*. 2011;6:2439-2443.
75. Chebib FT, Sussman CR, Wang X, Harris PC, Torres VE. Vasopressin and disruption of calcium signalling in polycystic kidney disease. *Nat Rev Nephrol*. 2015;11:451-464.
76. Chang M-Y, Lu J-K, Tian Y-C, et al. Inhibition of the P2X7 receptor reduces cystogenesis in PKD. *J Am Soc Nephrol*. 2011;22:1696-1706.
77. Kraus A, Grampp S, Goppelt-Struebe M, et al. P2Y2R is a direct target of HIF-1α and mediates secretion-dependent cyst growth of renal cyst-forming epithelial cells. *Purinergic Signal*. 2016;12:687-695.
78. Faria D, Schreiber R, Kunzelmann K. CFTR is activated through stimulation of purinergic P2Y2 receptors. *Pflugers Arch*. 2009;457:1373-1380.
79. Schreiber R, Buchholz B, Kraus A, et al. Lipid peroxidation drives renal cyst growth in vitro through activation of TMEM16A. *J Am Soc Nephrol*. 2019;30:228-242.
80. Bhaskaracharya A, Dao-Ung P, Jalilian I, et al. Probenecid blocks human P2X7 receptor-induced dye uptake via a pannexin-1 independent mechanism. *PLoS One*. 2014;9:e93058.
81. Poudel N, Okusa MD. Pannexins in acute kidney injury. *Nephron*. 2019;143:158-161.
82. EFSA Panel on Food Additives and Nutrient Sources added to Food (ANS). Scientific Opinion on the re-evaluation of Brilliant Blue FCF (E 133) as a food additive. *EFSA Journal*. 2010;8:1853-1889.

SUPPORTING INFORMATION

Additional Supporting Information may be found online in the Supporting Information section.

How to cite this article: Verschuren EHJ, Rigalli JP, Castenmiller C, et al. Pannexin-1 mediates fluid shear stress-sensitive purinergic signaling and cyst growth in polycystic kidney disease. *The FASEB Journal*. 2020;34:6382–6398. https://doi.org/10.1096/fj.201902901R